energies

MDPI

Article

Bi-Level Optimal Capacity Planning of Load-Side Electric Energy Storage Using an Emission-Considered Carbon Incentive Mechanism

Jieran Feng and Hao Zhou *

College of Electrical Engineering, Zhejiang University, Hangzhou 310027, China; jieran_feng@zju.edu.cn
* Correspondence: zhouhao_ee@zju.edu.cn

Abstract: The decarbonization of the power system forces the rapid development of electric energy storage (EES). Electricity consumption is the fundamental driving force of carbon emissions in the power system. However, the current EES capacity planning research that considers the load-side carbon emission responsibility is still limited. To fill this research gap, this paper proposes a carbon incentive mechanism while considering load-side carbon emission responsibility. Additionally, a bi-level optimal capacity planning model of the load-side EES based on carbon emission flow (CEF) theory is proposed. The upper level obtained the bus carbon intensities through the optimal economic dispatch and passed them to the lower level. Considering the carbon incentive mechanism, the lower level optimized the EES capacity. Finally, the model was tested by MATLAB/Gurobi in the modified IEEE-39 bus power system. The results show that under the stimulation of the carbon incentive mechanism, the bi-level optimal capacity planning model of the load-side EES could effectively promote peak shaving, valley filling, and carbon reduction. Furthermore, compared with the two existing EES subsidy policies, the proposed carbon incentive mechanism is verified to be more conducive to reducing system carbon emissions.

Keywords: capacity planning; carbon emission flow; carbon incentive mechanism; electric energy storage; load-side carbon emission responsibility; power system

Citation: Feng, J.; Zhou, H. Bi-Level Optimal Capacity Planning of Load-Side Electric Energy Storage Using an Emission-Considered Carbon Incentive Mechanism. *Energies* **2022**, *15*, 4592. https://doi.org/10.3390/en15134592

Academic Editor: Ahmed Abu-Siada

Received: 20 May 2022
Accepted: 21 June 2022
Published: 23 June 2022

1. Introduction

To meet the Paris Agreement temperature goal, reducing carbon emissions is more and more urgent [1–3]. The power system has tremendous technological potential for decarbonization [4,5]. Vigorously developing renewable energy technologies is an important way to realize the low-carbon transformation of the power system [5,6]. Under this trend, the development of energy storage systems is necessary [7,8]. With the advantages of a stable output and an energy time-shift, energy storage cooperates with intermittent renewable energy sources to form a good combination [6,9]. Therefore, the energy storage technology has become a research hotspot in the field of low-carbon energy, attracting extensive attention from international scholars [10–12].

At present, the industrial application of energy storage in China is still in the initial stage of development. Energy storage capacity planning has attracted a large amount of research. There have been numerous articles addressing different types of energy storage capacity planning. The existing research on electric energy storage (EES) capacity planning under different scenarios is sufficient [13–18]. In addition, there are also studies on capacity planning for thermal energy storage [19,20] and mechanical energy storage [21,22]. In recent years, the collaborative planning of hybrid energy storage capacity has become a new research point. An allocative method of hybrid electrical and thermal energy storage capacity based on seasonal differences is proposed in [23]. Hybrid energy storage capacity planning considering daily, weekly, and seasonal coordinate operations has also been studied [24]. However, the above studies only plan energy storage capacity from

the perspective of the energy system, without considering the carbon emissions of the energy system.

Some studies on source-side and grid-side energy storage planning have considered carbon emissions. Reference [25] incorporated the carbon emission penalty cost into the objective function in the planning of a multi-energy system that considered the thermal storage capacity of the heating network. In [26], the greenhouse gas emission reduction benefit was part of the objective function when jointly optimizing the capacities of distributed generating units and battery energy storage systems. However, since the impact of the load-side energy storage on carbon emission is indirect and difficult to estimate accurately, there are few studies on the load-side EES capacity planning that consider this factor.

Due to the high EES investment cost and insufficient peak-to-valley electricity price difference, the incentive policy is an important factor to be considered in load-side EES capacity planning. In China, current incentive policies for load-side EES mainly include two categories: the fiscal award and subsidy policy, and the preferential tax policy [27]. However, the above policies only drive the EES configuration and operation from an economic perspective and promote carbon reduction indirectly. The policies directly acting on the carbon reduction effect of load-side EES have not been researched. The proposed carbon emission flow (CEF) theory provides a good research approach for measuring load-side carbon emission responsibility [28,29], which makes an incentive policy directly acting on the carbon reduction effect of the load-side EES possible. Based on the CEF theory, this paper proposes a carbon incentive mechanism to realize the carbon-oriented ESS capacity planning. The carbon reduction and economic effect of the EES configuration under the carbon incentive mechanism are worthy of further study.

To fill the research gap, this paper incorporates the load-side carbon emission responsibility into the EES capacity planning process and thus proposes a carbon incentive mechanism. Additionally, a bi-level optimal capacity planning model of the load-side EES based on the CEF theory is proposed. Through the case studies, the effectiveness of the proposed mechanism in the bi-level planning model is verified. A comparative analysis is carried out between the proposed carbon incentive mechanism and the existing energy storage policies of discharge subsidy and capacity subsidy. Through analysis, it can be seen that the proposed carbon incentive mechanism has significant advantages in terms of both economics and carbon reduction. The main contributions of this paper are as follows:

(1) Based on the carbon emission flow theory, this paper proposes a bi-level optimal capacity planning model for the load-side EES that considers the load-side carbon emission responsibility.
(2) Focusing on carbon emissions of the power system, a carbon incentive mechanism of the load-side EES is proposed to promote the carbon-oriented EES configuration and operation.
(3) Through case analysis, the effectiveness of the bi-level EES capacity planning model with the carbon incentive mechanism is verified. Furthermore, compared with the two existing EES subsidy policies, the proposed carbon incentive mechanism has relative superiority in terms of both economics and carbon reduction.

The structure of this paper is arranged as follows: Section 2 introduces the carbon incentive mechanism based on the CEF theory, Section 3 introduces the bi-level optimal capacity planning model of the load-side EES, case studies are carried out in Section 4, and Section 5 summarizes the research work of this paper.

2. Carbon Incentive Mechanism Based on Carbon Emission Flow Theory

To achieve the goal of planning and operating low-carbon power systems, countries around the world have introduced a series of subsidy policies to promote the configuration of the EES to improve the consumption of the renewable energy. Currently, in China, subsidy policies based on the discharged electricity and the EES capacity are widely implemented. However, these policies lack a "carbon perspective" and cannot guide the EES capacity planning and operation strategy more directly and effectively to reduce

carbon emissions. Therefore, a carbon incentive mechanism based on the CEF theory is proposed in this paper. The proposed mechanism forms a time-of-use incentive according to the historical load-side carbon responsibility. The load-side carbon responsibility can be clarified by tracing the carbon emission flow, which is a virtual flow attached to the power flow as Figure 1 [30].

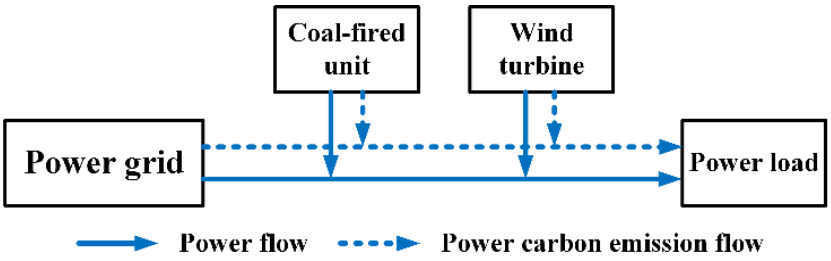

Figure 1. Schematic of the power flow and carbon emission flow.

2.1. CEF in Power System Considering Grid Losses

To accurately calculate the load-side carbon emission responsibility, the carbon emissions resulting from power transmission losses should not be neglected, as the power system grid loss rate can reach as high as 9% [31]. Therefore, a CEF model that considers grid losses is adopted in this paper. According to the method introduced in [30,32], the calculation method of the carbon emission flow is shown in Figure 2.

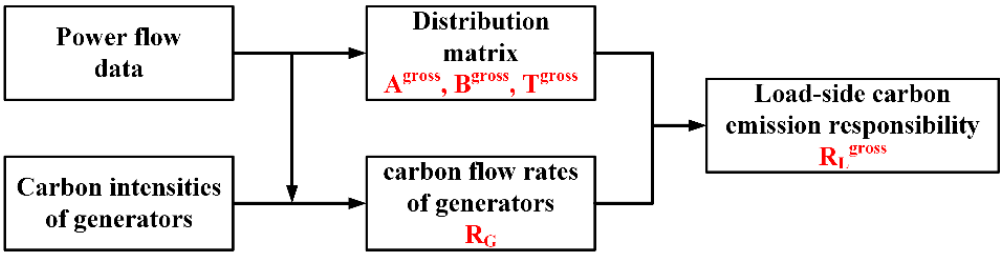

Figure 2. Schematic of the CEF calculation method.

To determine the distribution matrixes that account for grid losses, we define a gross bus power flux $P_{B,i}^{gross}$ as a total power flow through bus i which satisfies Kirchhoff's Current Law and which would flow if the network was fed with the actual generation and no power was lost in the network. It can be expressed as:

$$P_{B,i}^{gross} = \sum_{j \in i^+} P_{ji}^{gross} + P_{G,i} \tag{1}$$

where P_{ji}^{gross} is the gross flow in branch $i-j$ which would flow if no power was lost, which is defined as: $P_{ij}^{gross} = P_{ji} + P_{ij}^{loss}$; P_{ij}^{loss} is the grid losses on the branch $j-i$. P_{ji} denotes the active power from j to i on the branch $j-i$; i^+ denotes the starting bus set of the branch injected into bus i; P_{Gi} is the output power of the generator at bus i. Based on (1), we define a distribution matrix $\boldsymbol{A}^{gross}$ as:

$$A_{ij}^{gross} = \begin{cases} P_{ji}^{gross} / P_{B,i}^{gross} & j \in i^+ \\ 0 & else \end{cases} \tag{2}$$

Equation (3) can be derived from (1) and (2):

$$\boldsymbol{P}_B = (\boldsymbol{E}^{gross} - \boldsymbol{A}^{gross})^{-1} \boldsymbol{P}_G \tag{3}$$

where $\boldsymbol{P}_B$ represents the power flux column vector of n buses in the system; $\boldsymbol{E}^{gross}$ denotes the n-dimensional identity matrix; correspondingly, we define the distribution matrix $\boldsymbol{B}^{gross}$ as:

$$B_{ij}^{gross} = \begin{cases} P_{L,i}/P_{B,i}^{gross} & i = j \\ 0 & i \neq j \end{cases} \tag{4}$$

Based on (4), we can obtain:

$$\boldsymbol{P}_L^{gross} = \boldsymbol{B}^{gross}\boldsymbol{P}_B \tag{5}$$

where $\boldsymbol{P}_L^{gross}$ represents the column vector of the equivalent load of n nodes considering grid loss allocation.

From (3) and (5), we can get:

$$\boldsymbol{P}_L^{gross} = \boldsymbol{B}^{gross}(\boldsymbol{E}^{gross} - \boldsymbol{A}^{gross})^{-1}\boldsymbol{P}_G = \boldsymbol{T}^{gross}\boldsymbol{P}_G \tag{6}$$

where $\boldsymbol{T}^{gross}$ denotes a source-to-load power distribution matrix.

The carbon emission responsibility of generators per hour can be defined as $\boldsymbol{R}_G$, and each element of it can be expressed as:

$$R_{G,i} = e_{G,i}P_{G,i} \tag{7}$$

where $e_{G,i}$ denotes the carbon intensity of the generator at bus i. According to (6), we have:

$$\boldsymbol{R}_L^{gross} = \boldsymbol{T}^{gross}\boldsymbol{R}_G \tag{8}$$

where $\boldsymbol{R}_L^{gross}$ represents the vector of the load-side carbon emission responsibility. The carbon intensity of bus i can be expressed as:

$$e_i^{gross} = R_{L,i}^{gross}/P_{B,i}^{gross} \tag{9}$$

2.2. Carbon Incentive Mechanism

The load-side EES configuration and operation strategy formulation is essentially a nonrigid demand response without accounting for changes in the energy-consuming behavior. Currently, the load-side EES configuration and operation are normally driven by the time-of-use tariff and subsidy policies of the government only from the electrical perspective. Due to the character of the power system, in which sources depend on loads, the carbon emission responsibility is caused by the energy consumption of loads. Therefore, load-side carbon responsibility allocated from the source-side by the CEF theory can inform the load-side of the carbon emissions caused by their energy consumption and be adopted as the signal to drive the load-side EES configuration and operation [33]. From the emission-considered perspective, a carbon incentive mechanism is proposed to achieve low-carbon load-side EES configuration and operation.

Analogous to the time-of-use tariff, the carbon incentive mechanism should use different incentive coefficients in different periods; this would be to facilitate the discharging of the EES in the period of high carbon emissions and charging in the period of low carbon emission. The current peak-valley electricity price difference is not enough to make energy storage profitable, so in general, the carbon incentive mechanism should be presented as a subsidy for the loads necessary to promote energy storage configuration. The proposed carbon incentive mechanism includes the following three parts:

- Based on the CEF theory, calculate the historical load-side carbon responsibilities according to historical power flow data and adopt the average value of the historical load-side carbon responsibilities as the baseline.
- Compare the historical load-side carbon responsibilities with the baseline and form a time-of-use carbon incentive price. If the historical load-side carbon responsibility

is higher than the baseline, a high incentive price is adopted. If the historical carbon responsibility is lower than the baseline, a low incentive price is adopted.

- According to the incentive price, the carbon emission intensity of each load, and the actual discharge and charge electricity of the EES, the carbon incentive cost of each load can be obtained.

The subsidy under the carbon incentive mechanism is based on the contribution of an EES to carbon reduction. The total carbon incentive subsidy of load i can be expressed as:

$$C_i^{CI} = \sum_{t=1}^{T} p_t^{CI} e_{i,t}^{gross} P_{i,t}^{EES} \Delta t \tag{10}$$

where p_t^{CI} represents the carbon incentive price at time t. $P_{i,t}^{EES}$ represents the charged power of the *EES* if it is negative and the discharged power if positive. Δt represents the time step. The proposed carbon incentive mechanism is bi-directional and the punishment caused by charging will be deducted from the total subsidy.

3. Bi-Level Optimal Capacity Planning Model of the EES

3.1. Model Overview

The structure of the proposed bi-level optimal capacity planning model is shown in Figure 3. The upper-level conducts economic dispatch for the power transmission network and obtains the carbon intensity of buses, which can be regarded as a regional load aggregate, based on the CEF theory. The lower level takes the bus carbon intensity as the boundary condition, and the optimal EES capacity configuration of each bus can be obtained and passed back to the upper level. The process iterates until the results stabilize.

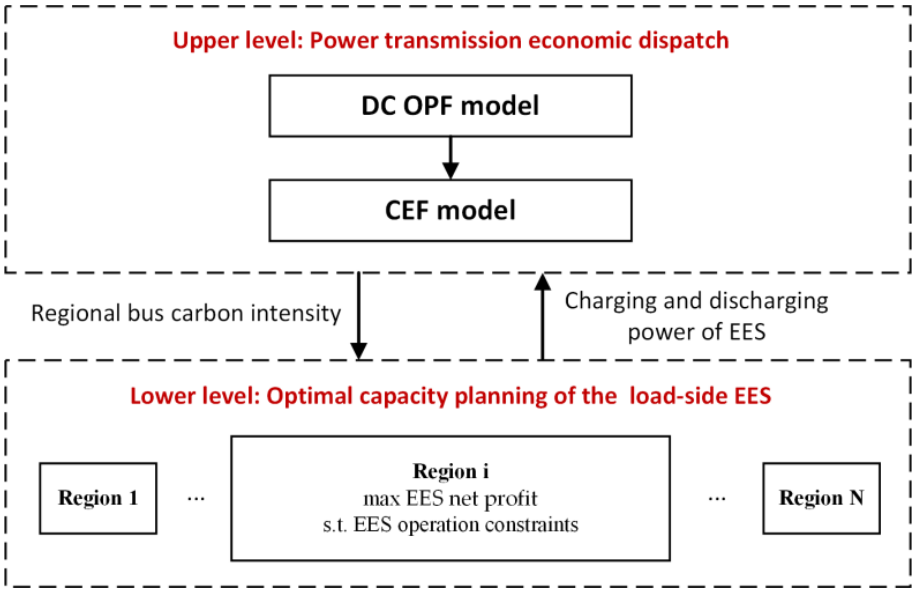

Figure 3. Structure of the bi-level model.

3.2. The Upper Level: Economic Dispatch Model

3.2.1. Optimization Objective

The upper-level model performs an economic dispatch to minimize the cost of power generation. Equation (11) is the objective function of the upper level and represents the total power generation cost.

$$min \sum_{t=0}^{T} \left(\sum_{CG=1}^{N_{CG}} c_{CG} P_t^{CG} + \sum_{GG=1}^{N_{GG}} c_{GG} P_t^{GG} + \sum_{WT=1}^{N_{WT}} c_{WT} P_t^{WT} \right) \tag{11}$$

where c_{CG}, c_{GG}, and c_{WT} represent the power generation cost coefficients for coal-fired generators, gas-fired generators, and wind turbines, respectively; P_t^{CG}, P_t^{GG}, and P_t^{WT} represent the power output of coal-fired generators, gas-fired generators, and wind turbines at time t, respectively; N_{CG}, N_{GG}, and N_{WT} represent the number of coal-fired generators, gas-fired generators, and wind turbines in the system, respectively; T represents the model calculation period.

3.2.2. Constraints

This paper adopts the DC power flow model to consider grid losses for the power system [34]. Equations (12)–(20) represent the operational constraints of the power system. Specifically, inequalities (12)–(14) represent generator output constraints. Equations (15) and (16) represent branch power flow and grid loss constraints. Inequality (17) represents the branch power flow transmission capacity constraint. Equation (18) is the bus power balance constraint. Inequality (19) is used to constrain the phase angle difference of each branch within a reasonable range. Equation (20) is the slack bus phase angle constraint.

$$P_{min}^{CG} \le P_t^{CG} \le P_{max}^{CG} \tag{12}$$

$$P_{min}^{GG} \le P_t^{GG} \le P_{max}^{GG} \tag{13}$$

$$P_{min}^{WT} \le P_t^{WT} \le P_{max}^{WT} \tag{14}$$

$$P_{ij,t} = \frac{\theta_{ij,t}}{x_{ij}} \tag{15}$$

$$P_{ij,t}^{loss} = g_{ij} \theta_{ij,t}^2 \tag{16}$$

$$P_{ij,min} \le P_{ij} \le P_{ij,max} \tag{17}$$

$$P_i^{CG} + P_i^{GG} + P_i^{WT} = \sum_{j \in \Omega_i} P_{ij} + \sum_{j \in \Omega_i} \frac{1}{2} P_{ij}^{loss} + P_i^{load} \tag{18}$$

$$\theta_{ij,min} \le \theta_{ij,t} \le \theta_{ij,max} \tag{19}$$

$$\theta_{ref,t} = 0 \tag{20}$$

where P_{max}^{CG} and P_{min}^{CG} denote the maximum and minimum output power of coal-fired generators, respectively; P_{max}^{GG} and P_{min}^{GG} denote the maximum and minimum output power of gas-fired generators, respectively; P_{max}^{WT} and P_{min}^{WT} denote the maximum and minimum output power of wind turbines, respectively; $\theta_{ij,t}$, x_{ij}, and g_{ij} represent the phase angle difference, reactance, and conductance of branch $i-j$, respectively; $P_{ij,t}$ and $P_{ij,t}^{loss}$ denote the transmission power and losses of branch $i-j$, respectively; $P_{ij,max}$ and $P_{ij,min}$ denote the maximum and minimum transmission power of branch $i-j$, respectively; P_i^{CG}, P_i^{GG}, and P_i^{WT} denote the power injection; P_i^{load} denotes the power demand of bus i; Ω_i denotes the set of buses connected to bus i; $\theta_{ij,max}$ and $\theta_{ij,min}$ denote the maximum and minimum phase angle difference of branch $i-j$; $\theta_{ref,t}$ denotes the phase angle at the slack bus.

3.3. The Lower Level: EES Capacity Planning Model

3.3.1. Optimization Objective

The lower-level optimization model plans the energy storage capacity configured on the load buses. The objective is to maximize the EES net profit as (21). Specifically, the cost of the EES includes the investment cost and operation and maintenance cost as (24) and (25), and the benefit of the EES includes time-of-use tariff arbitrage income as (22),

the carbon incentive mechanism subsidy as (10), and the recyclable value of EES devices as (23).

$$max \sum_{i=1}^{N_{EES}} \left(C_i^{ele} + C_i^{CI} + C_i^{rec} - C_i^{inv} - C_i^{ope} \right) \tag{21}$$

$$C_i^{ele} = \sum_{t=1}^{\mathrm{T}} p_t^{ele} \left(P_{i,t}^{cha} - P_{i,t}^{dis} \right) \Delta t \tag{22}$$

$$C_i^{rec} = \gamma_{rec} C_i^{inv} \tag{23}$$

$$C_i^{inv} = \frac{c_E^{ESS} E_{N,i}^{ESS} + c_P^{ESS} P_{N,i}^{ESS}}{365 \times 24 N_Y} T \tag{24}$$

$$C_i^{ope} = \frac{\sum_{n=1}^{N_Y} c_{ope} E_{N,i}^{ESS} \left(\frac{1+i_r}{1+d_r} \right)^n}{365 \times 24 N_Y} T \tag{25}$$

where C_i^{ele} represents the benefit of energy storage by reducing electricity purchase costs in period T; C_i^{CI} represents the total subsidy of the carbon incentive mechanism as shown in (10); C_i^{rec} represents the recycling value of the EES devices; C_i^{inv} represents the average cost of EES investment in period T; C_i^{ope} represents the average cost of EES operation and maintenance in period T; c_E^{ESS} and c_P^{ESS} represent the per unit investment cost of the EES capacity and rated power; $E_{N,i}^{ESS}$ and $P_{N,i}^{ESS}$ represents the optimal EES storage capacity and rated power of ESS_i; N_Y represents the service life of the EES; c_{ope} represents the per-unit cost of operation and maintenance; i_r and d_r represent the inflation rate and discount rate; $P_{i,t}^{cha}$ and $P_{i,t}^{dis}$ represent the charging and discharging power of EES_i at time t, respectively; p_t^{ele} represents the electricity purchase price at time t; γ_{rec} represents the recyclable value rate.

3.3.2. Constraints

Energy storage modeling includes energy and power constraints, as shown in Equations (26)–(33). Equation (26) denotes the relationship between the state of charge (SOC) of the EES at time $t+1$ and time t. Equation (27) indicates that the SOC of the EES is equal at the beginning and end of the planning period. Inequalities (28)–(30) are the upper and lower limits of the SOC, charging power, and discharging power of the EES at time t, respectively. Constraints (31)–(32) are used to ensure that the EES does not charge and discharge at the same time. Equation (33) denotes the relationship between the rated capacity and rated power of the EES.

$$E_{t+1} = (1 - \gamma_{loss}) E_t + \left(\eta_{cha} P_t^{cha} - P_t^{dis} / \eta_{dis} \right) \cdot \Delta t \tag{26}$$

$$E_0 = E_T \tag{27}$$

$$\alpha_{min} E_N \le E_t \le \alpha_{max} E_N \tag{28}$$

$$0 \le P_t^{cha} \le B_t^{cha} P_N \tag{29}$$

$$0 \le P_t^{dis} \le B_t^{dis} P_N \tag{30}$$

$$0 \le B_t^{cha} + B_t^{dis} \le 1 \tag{31}$$

$$B_t^{cha}, B_t^{dis} \in \{0, 1\} \tag{32}$$

$$\Gamma = E_N / P_N \tag{33}$$

where E_t represents the SOC of the EES at time t; γ_{loss} represents the self-discharge rate of the EES; η_{cha} and η_{dis} represent charging efficiency and discharging efficiency, respectively; E_N and P_N represent the optimal rated capacity and rated power of the EES, respectively; α_{max} and α_{min} represent the upper and lower limit coefficients of EES charge and discharge

depth, respectively; B_t^{cha} and B_t^{dis} are Boolean variables used to represent the state of charge and discharge of the EES at time t, respectively; Γ represents the rated time of the EES.

To convert the model to a mixed integer linear programming (MILP) problem, $B_{cha,t}P_N$ and $B_{dis,t}P_N$ in Equations (29) and (30) need to be linearized. Let $P_N^{cha} = B_t^{cha}P_N$ and $P_N^{dis} = B_t^{dis}P_N$, then inequalities (29) and (30) can be linearized to (34)–(38) and (39)–(43), respectively, based on the big-M method.

$$0 \le P_t^{cha} \le P_N^{cha} \tag{34}$$

$$P_N^{cha} \le MB_t^{cha} \tag{35}$$

$$P_N^{cha} \ge 0 \tag{36}$$

$$P_N^{cha} \le P_N \tag{37}$$

$$P_N^{cha} \ge P_N - M\left(1 - B_t^{cha}\right) \tag{38}$$

$$0 \le P_t^{dis} \le P_N^{dis} \tag{39}$$

$$P_N^{dis} \le MB_t^{dis} \tag{40}$$

$$P_N^{dis} \ge 0 \tag{41}$$

$$P_N^{dis} \le P_N \tag{42}$$

$$P_N^{dis} \ge P_N - M\left(1 - B_t^{dis}\right) \tag{43}$$

4. Case Study

To verify the effectiveness and superiority of the proposed model, a modified IEEE 39-bus power system was employed as the test object. The optimization results of the proposed bi-level model are discussed, and the carbon reduction effects of the proposed mechanism and existing energy storage subsidy policies are compared.

4.1. Test System and Initial Parameters

The modified power system is shown as Figure 4. The power system included six coal-fired units, three wind turbine units, and two gas-fired units. The parameters of units are shown in Table 1 [35,36]. The detailed data of each power load are shown in Table 2. According to the actual electricity price of a city in eastern China, the parameters of the time-of-use tariff are shown in Table 3. Four typical days of four seasons, aggregated to 96 h in seasonal order with 1 h time resolution, were employed as the EES optimal capacity planning period. Similarly to other studies [37,38], typical data of four-season wind turbine output were used as initial parameters. The per-unit values of 24-h wind turbine output and power demand of each four-season typical day are shown in Figures 5 and 6, respectively. The wind turbine capacities in Table 1 and maximum power loads in Table 2 were adopted as base values, respectively. The coefficients of the carbon incentive mechanism are shown in Table 4. The iron-lithium battery was chosen as the EES in this study, and its parameters are shown in Table 5 [39,40]. Case studies were carried out on the MATLAB/YALMIP platform by adopting Gurobi solver.

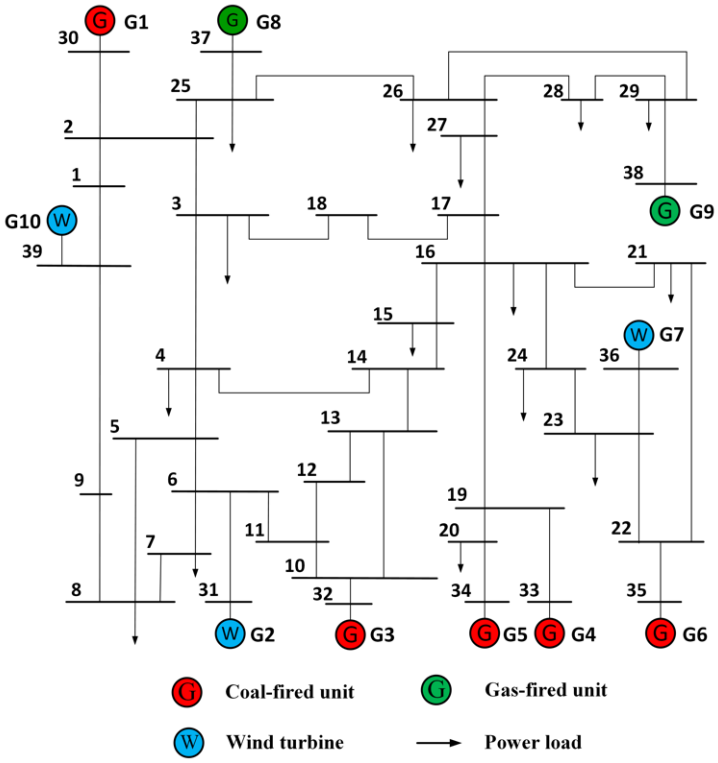

Figure 4. Modified IEEE 39-bus power system.

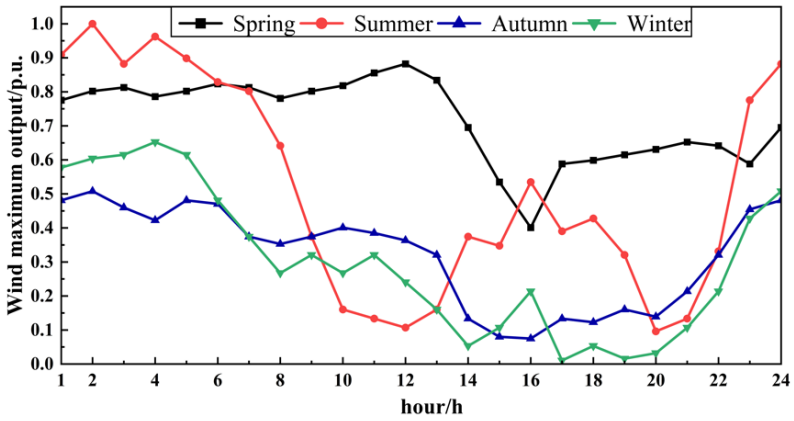

Figure 5. Wind maximum of four-season typical days.

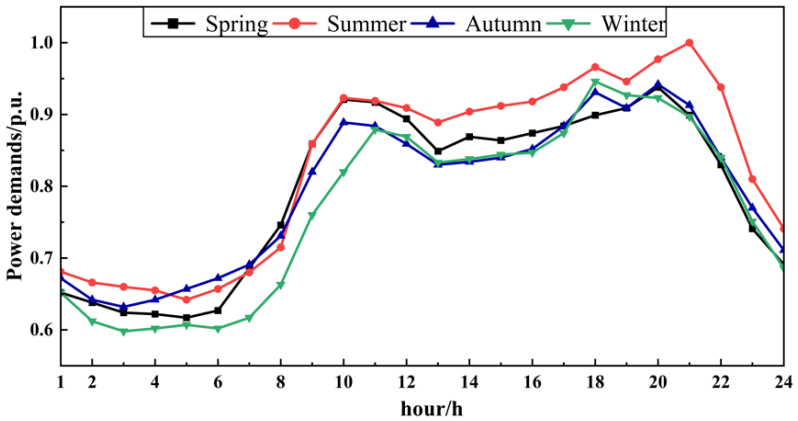

Figure 6. Power demand of four-season typical days.

Table 1. Parameters of power units.

Unit	Type	Capacity (MW)	Cost Coefficient ($/MWh)	Emission Intensity (tCO_2/MWh)
G1	Coal-fired	1040	35	1.303
G2	Wind turbine	725	15	0.006
G3	Coal-fired	925	35	1.303
G4	Coal-fired	852	35	1.303
G5	Coal-fired	908	35	1.303
G6	Coal-fired	887	35	1.303
G7	Wind turbine	725	15	0.006
G8	Gas-fired	564	62	0.564
G9	Gas-fired	865	62	0.564
G10	Wind turbine	725	15	0.006

Table 2. Parameters of Power Loads.

Bus	Power Load (MW)	Bus	Power Load (MW)
3	322	23	247.5
4	500	24	308.6
7	233.8	25	224
8	522	26	139
15	320	27	281
16	329	28	206
20	680	29	283.5
21	274	/	/

Table 3. Parameters of Time-of-use Tariffs.

Period	Electricity Price ($/kWh)
0:00~8:00	0.036
8:00~22:00	0.126
22:00~24:00	0.036

Table 4. Coefficients of the Carbon Incentive Mechanism.

Period	Coefficient ($/$tCO_2$)
period of higher carbon emission responsibility	5
period of lower carbon emission responsibility	3

Table 5. Parameters of the EES.

Parameter	Value	Parameter	Value
Unit power cost	100 $/kW	Charge depth	90%
Unit capacity cost	250 $/kWh	Discharge depth	10%
Operation cost	25 $/(kW·Year)	Recyclable value rate	10%
Service life	8 Years	Inflation rate	2%
Charge/discharge efficiency	95%	Discount rate	10%

4.2. Optimization Results of EES Capacity Configuration

Based on the CEF theory, the carbon emission responsibilities of each power load were calculated according to the historical data of four-season typical days. Taking the power load in bus 3 as an example, its 96-h carbon emission responsibility is shown in Figure 7. As shown in Figure 7, the blue solid line represents the carbon emission responsibility of power load in bus 3, and the red dotted line represents the average value of its 96-h

carbon emission responsibility. In typical spring days, the maximum wind output during the daytime is higher than in the other three seasons. According to the carbon incentive mechanism proposed in Section 2, when the carbon emission responsibilities are above the average value, a high carbon incentive coefficient is applied. When the carbon emission responsibilities are below the average value, a low carbon incentive coefficient is applied.

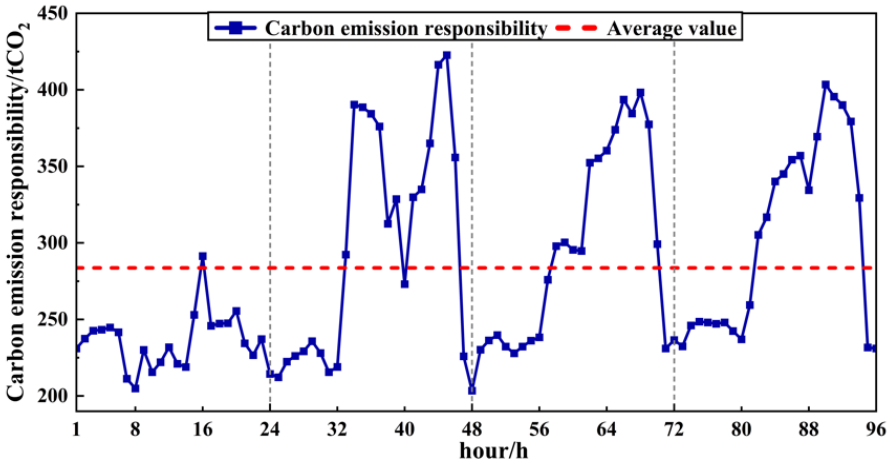

Figure 7. Carbon emission responsibility and average value.

For blank control, we analyzed the unsubsidized case and the case considering the proposed carbon incentive mechanism. The comparisons of energy supply cost, subsidy, and total capacity configuration of the EES are shown in Table 6. The EES capacity configurations of each load are shown in Figure 8.

Table 6. The Comparisons of Energy Supply Cost, Subsidy, and Capacity Configuration.

Case	Energy Supply Cost (10^7\$)	Subsidy (10^5\$)	Capacity Configuration of EES (MWh)
Unsubsidized case	1.201	0	0
Proposed method	1.174	1.071	6564.9

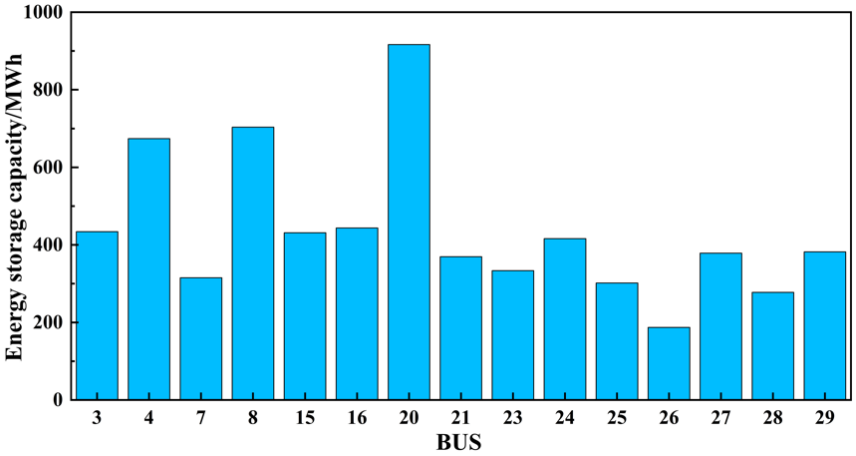

Figure 8. EES capacity configuration after the EES configuration.

As shown in Table 6, when there is no subsidy, the EES will not be configured, as the current time-of-use tariff arbitrage income is not large enough. In the case considering the proposed method, the overall carbon incentive mechanism is shown as a subsidy to the power loads. In this way, the power loads are stimulated for EES configuration and the energy supply cost is correspondingly reduced.

After generating the bi-level planning model that considered the carbon incentive mechanism, the total power demand and carbon emission responsibility before and after the EES configuration were calculated; they are shown in Figures 9 and 10, respectively.

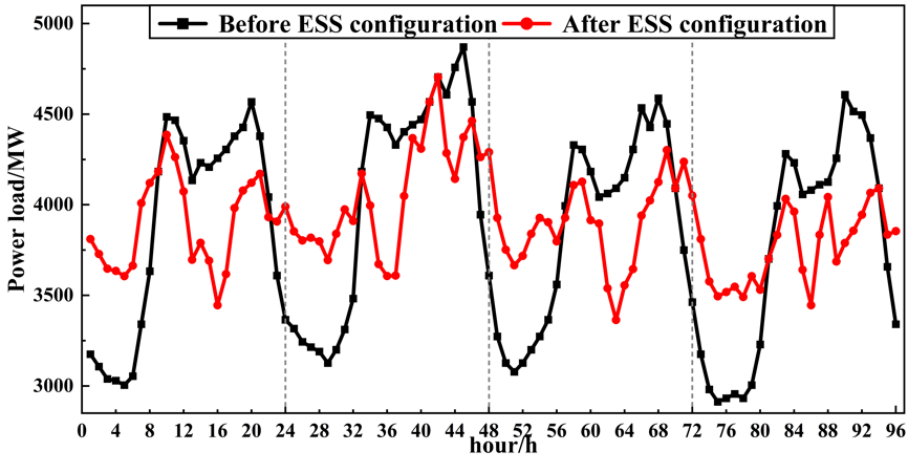

Figure 9. Total power demand before and after the EES configuration.

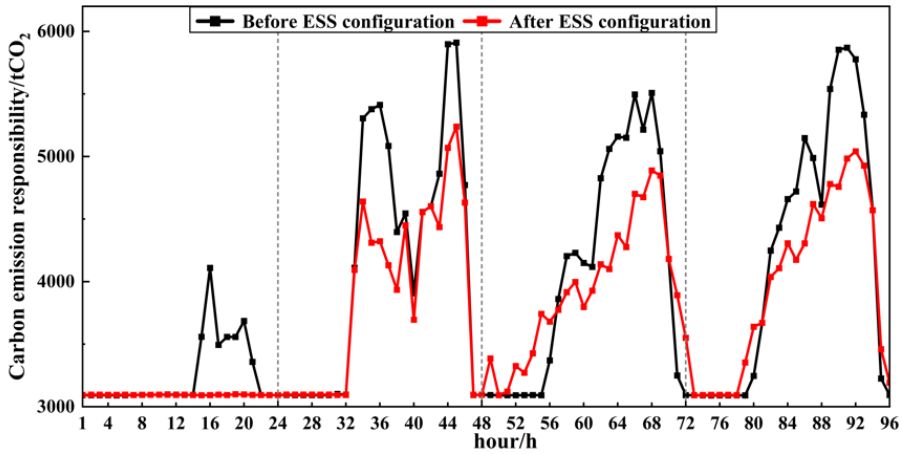

Figure 10. Total carbon emission responsibility before and after the EES configuration.

As can be seen from Figure 9, the model can effectively shave peaks and fill valleys for power loads by time-shifting the power demand with the EES. As shown in Figure 10, for original carbon emission responsibility, the curve is relatively stable every night. This was caused by two reasons: first, the minimum limit of thermal-power unit output caused the same fundamental carbon emission responsibility in each period; second, the excess power demand above the lower output limit of thermal power units at night was met by abundant wind power resources and would only cause extremely small carbon emissions. In a typical spring day, due to having the most abundant wind power resources of the four seasons, the peak of carbon emission responsibility was relatively low and could be fully shaved by time-shifting the power demand with EES. In typical spring and summer days, the time-shifted power demand to shave the carbon responsibility peak did not result in a significant increase in nighttime carbon emission responsibility. This is because the wind power resources in spring and summer are relatively abundant, and the time-shifted power demand may be fully met by wind power. Correspondingly, in typical autumn and winter days, the wind power resources are not abundant and the time-shifted power demand to shave the carbon responsibility peak results in a significant increase in nighttime carbon emission responsibility. As shown in Figure 10, total carbon emission responsibility is effectively reduced by 5.2% through the EES configuration.

The charge or discharge power and SOC of bus 3 are shown in Figure 11. The carbon emission responsibility before and after EES configuration is shown as Figure 12. As shown in Figure 11, the EES is generally charged at night and discharged in the daytime. Due to the time-of-use tariff, it is more economical to charge the EES at night and discharge it in the daytime. For the proposed carbon incentive mechanism, it is more cost-effective to discharge the EES when the carbon emission responsibility is higher than the average value, in order to achieve the effect of shaving carbon emission responsibility peaks.

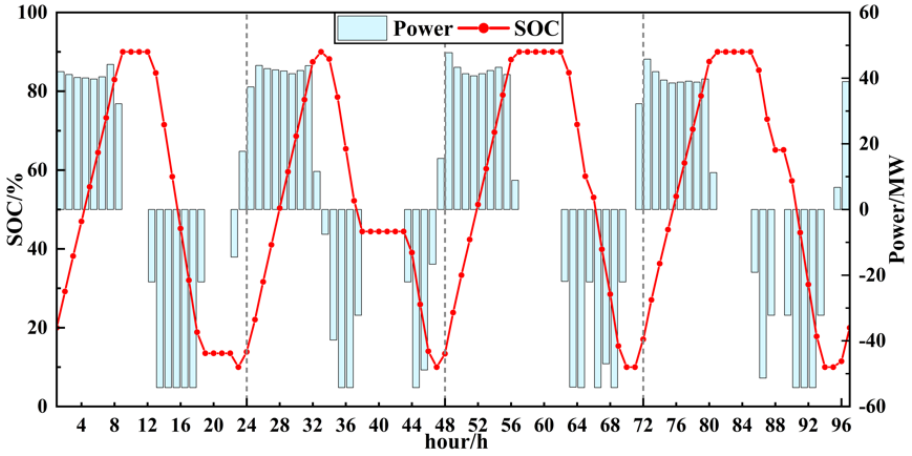

Figure 11. Optimal scheduling of the EES at Bus 3.

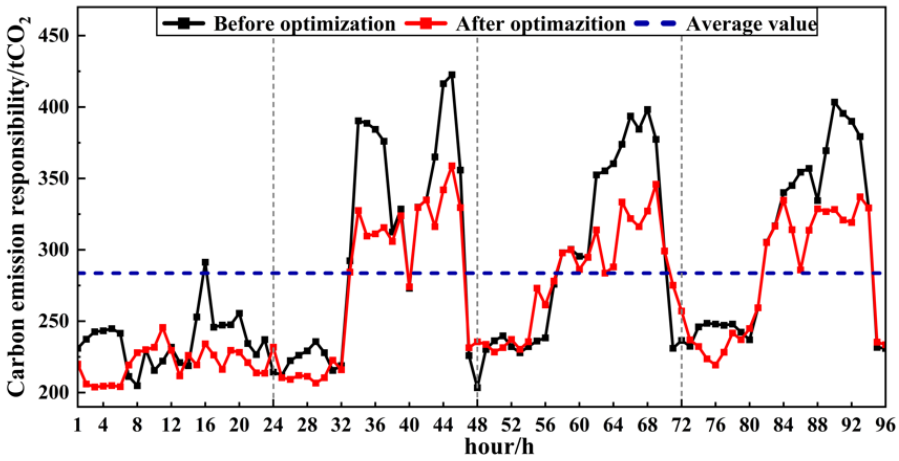

Figure 12. Carbon emission responsibility of the load at bus 3 before and after the EES configuration.

4.3. Comparison of the Proposed Mechanism with the Two Existing Policies

To demonstrate the superiority of the proposed mechanism, three different cases are compared.

- Case 1: Bi-level optimal capacity planning of the load-side EES with the proposed carbon incentive mechanism;
- Case 2: Bi-level optimal capacity planning of the load-side EES with a discharge subsidy policy;
- Case 3: Bi-level optimal capacity planning of the load-side EES with a capacity subsidy policy.

The two kinds of subsidy policies in Case 2 and Case 3 are widely used to promote energy storage configuration in China. For the discharge subsidy policy, the actual subsidy price is 15 $/MWh. For the capacity subsidy policy, the actual subsidy price is 23 $/MWh. Furthermore, to compare the three cases, different subsidy prices are considered. The

relationship between carbon reduction and total subsidy cost in three cases is shown in Figure 13.

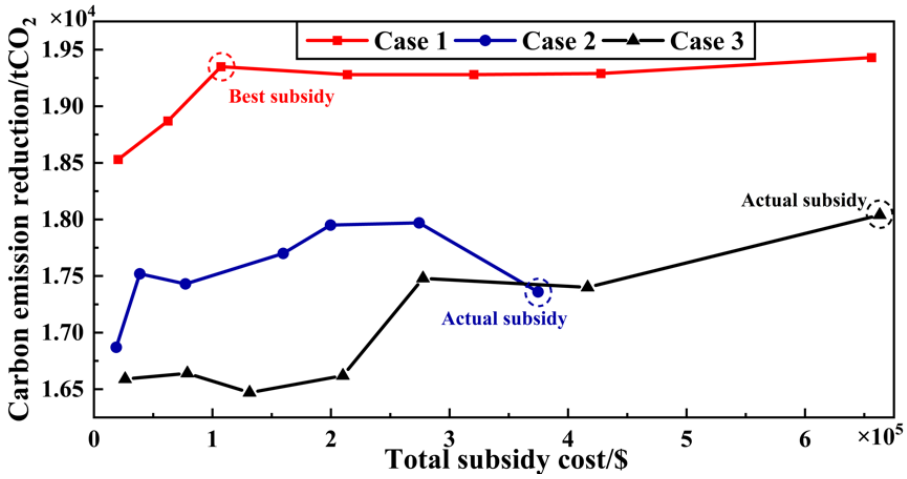

Figure 13. The relationship between carbon reduction and total subsidy cost in three cases.

As shown in Figure 13, as the total subsidy cost increased, the carbon reduction effect in three cases generally increased first and then stabilized. However, the carbon reduction effect of Case 2 slightly decreased in the case of the actual subsidy, because excessive discharge subsidies can cause unnecessary charging during high carbon periods. In general, with the same total subsidy cost, the carbon reduction effect of using the proposed carbon incentive mechanism was better than the other two subsidy policies. Specifically, when the subsidy costs of the proposed mechanism were about 1/4 of the actual discharge subsidy policy and 1/7 of the capacity subsidy policy, the carbon reduction effect could be increased by about 11.5% and 7.3%, respectively. Therefore, compared to the other two existing policies, the proposed mechanism can significantly promote the carbon reduction effect by directly guiding the EES to low-carbon-oriented operation.

The 96-h total power load and carbon emission responsibility in the three cases are shown in Figures 14 and 15, respectively. The power demand curves after the EES configuration in Case 2 and Case 3 are more volatile than it in Case 1. As elaborated in Section 4.2, the key to carbon reduction is to shift the power demand in carbon-peak periods to other periods with redundant wind power. Taking the load at bus 3 as an example, the SOCs of it in the three cases are shown in Figure 16 and the bus prices of bus 3 are shown in Figure 17. The bus price represents the unit electricity purchase cost of the bus after deducting the subsidy. For Case 2, the power load and carbon emission responsibility after the EES configuration were sometimes higher than those before the EES configuration. This is because, under the discharge subsidy policy, the EES were encouraged to discharge more to profit. The unnecessary charging and discharging during the daytime led to the weakening of the carbon reduction and peak shaving effects. For Case 3, as shown in Figures 14 and 15, the capacity subsidy policy did not facilitate the EES to shift the power demand in carbon-peak periods to other periods and therefore weakened the carbon reduction effect. To sum up, the proposed carbon incentive mechanism based on load-side carbon emission responsibility can effectively shift the power demand in carbon-peak periods to other periods with redundant wind power, thereby reducing carbon emissions.

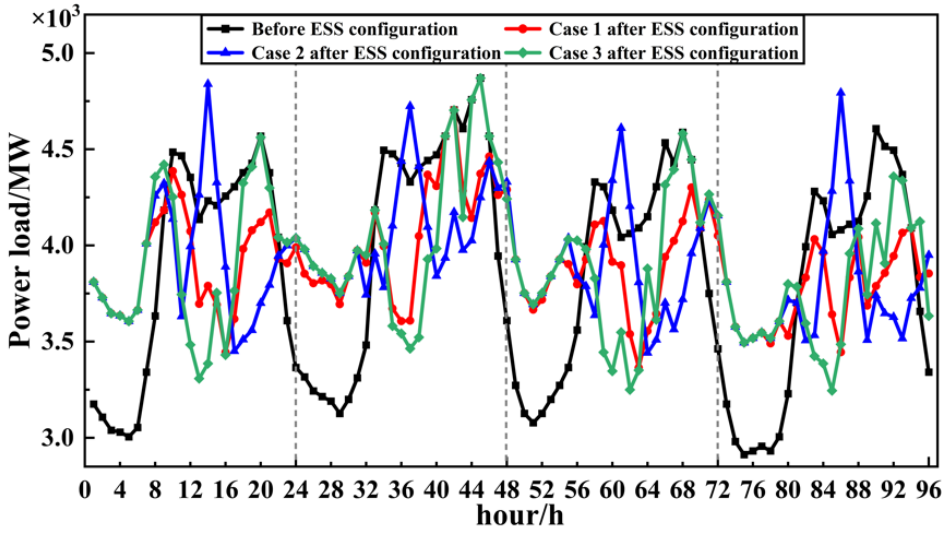

Figure 14. The total power load before and after the EES configuration in three cases.

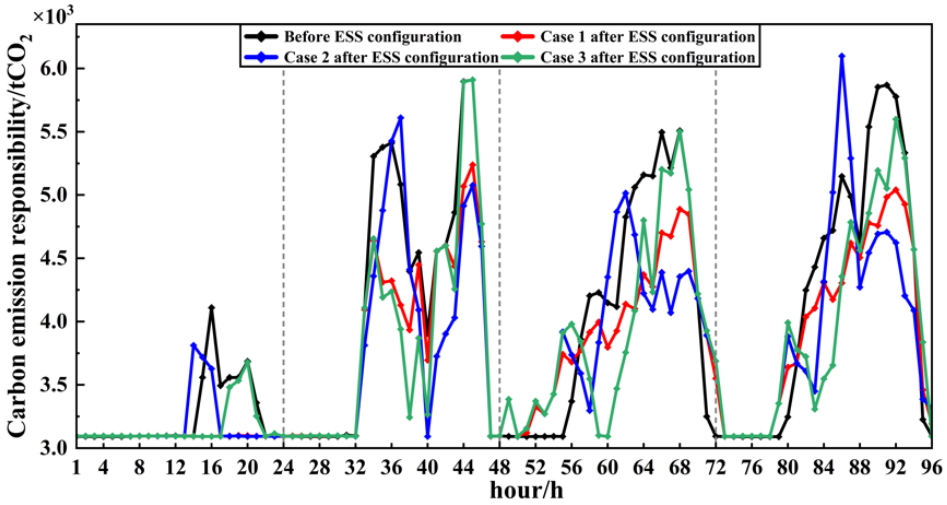

Figure 15. The total carbon emission responsibility before and after the EES configuration in three cases.

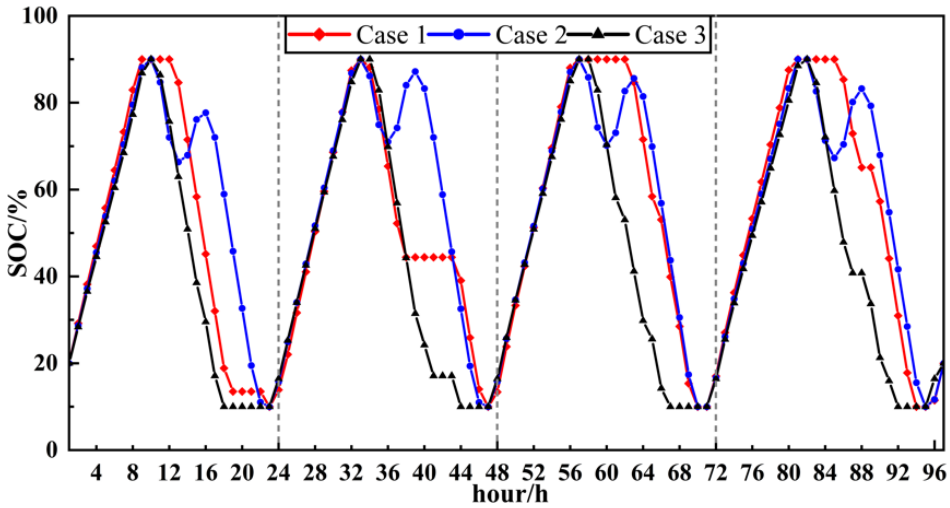

Figure 16. The SOC of the EES at Bus 3 in three cases.

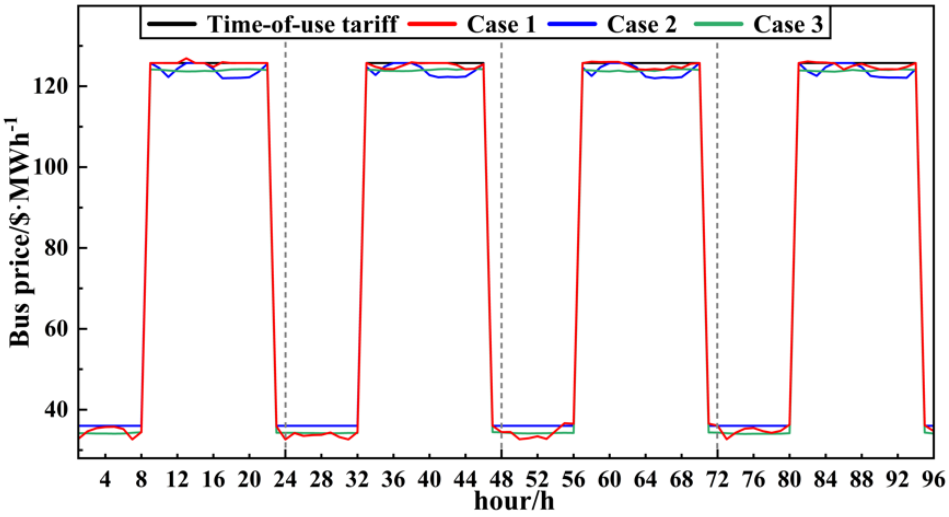

Figure 17. The bus prices of Bus 3 in three cases and the time-of-use tariff.

5. Conclusions

In this paper, a bi-level optimal capacity planning model of the load-side EES is proposed. In the upper level, the load bus carbon intensities were obtained based on the power economic dispatch and the CEF theory. In the lower level, a low-carbon optimal capacity planning model of the regional load-side EES was carried out with the objective of maximizing the net profit of the EES. Moreover, a carbon incentive mechanism was proposed and employed in the lower level to promote the configuration and operation of the load-side EES in a low-carbon direction. Cases based on the modified IEEE 39-bus power system were studied to test the effectiveness and superiority of the proposed bi-level model and the carbon incentive mechanism. The results show that the proposed bi-level model embedded with the carbon incentive mechanism can effectively guide the configuration and operation of the load-side EES, thereby promoting wind power consumption, realizing load peak shaving and valley filling, and reducing system carbon emission by 5.2%. Furthermore, compared with the two existing EES subsidy policies, the proposed carbon incentive mechanism has an obvious advantage in stimulating the EES carbon reduction. Specifically, when the subsidy costs of the proposed mechanism are about 1/4 of the actual discharge subsidy policy and 1/7 of the capacity subsidy policy, the carbon reduction effect can be increased by about 11.5% and 7.3%, respectively. This paper provides a reference for policymakers to formulate load-side carbon incentive policies to encourage the low-carbon configuration of energy storage.

This research serves as a starting point for further research into the impacts of carbon taxes and carbon trading on load-side energy storage planning.

Author Contributions: Conceptualization, J.F. and H.Z.; methodology, J.F. and H.Z.; software, J.F.; validation, H.Z.; formal analysis, J.F. and H.Z.; investigation, J.F.; resources, H.Z.; data curation, J.F., and H.Z.; writing—original draft preparation, J.F.; writing—review and editing, H.Z.; visualization, J.F.; supervision, H.Z.; project administration, H.Z. All authors have read and agreed to the published version of the manuscript.

Funding: This research received no external funding.

Institutional Review Board Statement: Not applicable.

Informed Consent Statement: Not applicable.

Data Availability Statement: The data that support the findings of this study are available from the corresponding author upon reasonable request.

Conflicts of Interest: The authors declare no conflict of interest.

References

1. Meinshausen, M.; Lewis, J.; McGlade, C.; Gutschow, J.; Nicholls, Z.; Burdon, R.; Cozzi, L.; Hackmann, B. Realization of Paris Agreement pledges may limit warming just below 2 degrees C. *Nature* **2022**, *604*, 304–309. [CrossRef] [PubMed]
2. Höhne, N.; Gidden, M.J.; den Elzen, M.; Hans, F.; Fyson, C.; Geiges, A.; Jeffery, M.L.; Gonzales-Zuñiga, S.; Mooldijk, S.; Hare, W.; et al. Wave of net zero emission targets opens window to meeting the Paris Agreement. *Nat. Clim. Chang.* **2021**, *11*, 820–822. [CrossRef]
3. Zhou, S.; Tong, Q.; Pan, X.; Cao, M.; Wang, H.; Gao, J.; Ou, X. Research on low-carbon energy transformation of China necessary to achieve the Paris agreement goals: A global perspective. *Energy Econ.* **2021**, *95*, 105137. [CrossRef]
4. Xiao, J.; Li, G.; Xie, L.; Wang, S.; Yu, L. Decarbonizing China's power sector by 2030 with consideration of technological progress and cross-regional power transmission. *Energy Policy* **2021**, *150*, 112150. [CrossRef]
5. Kang, J.-N.; Wei, Y.-M.; Liu, L.-C.; Han, R.; Yu, B.-Y.; Wang, J.-W. Energy systems for climate change mitigation: A systematic review. *Appl. Energy* **2020**, *263*, 114602. [CrossRef]
6. Jurasz, J.; Canales, F.A.; Kies, A.; Guezgouz, M.; Beluco, A. A review on the complementarity of renewable energy sources: Concept, metrics, application and future research directions. *Sol. Energy* **2020**, *195*, 703–724. [CrossRef]
7. Olabi, A.G.; Onumaegbu, C.; Wilberforce, T.; Ramadan, M.; Abdelkareem, M.A.; Al–Alami, A.H. Critical review of energy storage systems. *Energy* **2021**, *214*, 118987. [CrossRef]
8. Koohi-Fayegh, S.; Rosen, M.A. A review of energy storage types, applications and recent developments. *J. Energy Storage* **2020**, *27*, 101047. [CrossRef]
9. Basit, M.A.; Dilshad, S.; Badar, R.; Sami ur Rehman, S.M. Limitations, challenges, and solution approaches in grid-connected renewable energy systems. *Int. J. Energy Res.* **2020**, *44*, 4132–4162. [CrossRef]
10. Sepulveda, N.A.; Jenkins, J.D.; Edington, A.; Mallapragada, D.S.; Lester, R.K. The design space for long-duration energy storage in decarbonized power systems. *Nat. Energy* **2021**, *6*, 506–516. [CrossRef]
11. Groppi, D.; Pfeifer, A.; Garcia, D.A.; Krajačić, G.; Duić, N. A review on energy storage and demand side management solutions in smart energy islands. *Renew. Sustain. Energy Rev.* **2021**, *135*, 110183. [CrossRef]
12. Rahman, M.M.; Oni, A.O.; Gemechu, E.; Kumar, A. Assessment of energy storage technologies: A review. *Energy Convers. Manag.* **2020**, *223*, 113295. [CrossRef]
13. Shi, Z.; Wang, W.; Huang, Y.; Li, P.; Dong, L. Simultaneous Optimization of Renewable Energy and Energy Storage Capacity with the Hierarchical Control. *CSEE J. Power Energy Syst.* **2022**, *8*, 95–104.
14. Kumar, N.; Kumar, T.; Nema, S.; Thakur, T. A multiobjective planning framework for EV charging stations assisted by solar photovoltaic and battery energy storage system in coupled power and transportation network. *Int. J. Energy Res.* **2021**, *46*, 4462–4493. [CrossRef]
15. Yi, T.; Cheng, X.; Chen, Y.; Liu, J. Joint optimization of charging station and energy storage economic capacity based on the effect of alternative energy storage of electric vehicle. *Energy* **2020**, *208*, 118357. [CrossRef]
16. Karimi, A.; Aminifar, F.; Fereidunian, A.; Lesani, H. Energy storage allocation in wind integrated distribution networks: An MILP-Based approach. *Renew. Energy* **2019**, *134*, 1042–1055. [CrossRef]
17. Akram, U.; Khalid, M.; Shafiq, S. Optimal sizing of a wind/solar/battery hybrid grid-connected microgrid system. *IET Renew. Power Gener.* **2017**, *12*, 72–80. [CrossRef]
18. Dvorkin, Y.; Fernandez-Blanco, R.; Kirschen, D.S.; Pandzic, H.; Watson, J.-P.; Silva-Monroy, C.A. Ensuring Profitability of Energy Storage. *IEEE Trans. Power Syst.* **2017**, *32*, 611–623. [CrossRef]
19. Gou, X.; Chen, Q.; Hu, K.; Ma, H.; Chen, L.; Wang, X.-H.; Qi, J.; Xu, F.; Min, Y. Optimal planning of capacities and distribution of electric heater and heat storage for reduction of wind power curtailment in power systems. *Energy* **2018**, *160*, 763–773. [CrossRef]
20. Mansoor, M.; Stadler, M.; Zellinger, M.; Lichtenegger, K.; Auer, H.; Cosic, A. Optimal planning of thermal energy systems in a microgrid with seasonal storage and piecewise affine cost functions. *Energy* **2021**, *215*, 119095. [CrossRef]
21. Li, K.; Wei, X.; Yan, Y.; Zhang, C. Bi-level optimization design strategy for compressed air energy storage of a combined cooling, heating, and power system. *J. Energy Storage* **2020**, *31*, 101642. [CrossRef]
22. Xu, Y.; Lang, Y.; Wen, B.; Yang, X. An Innovative Planning Method for the Optimal Capacity Allocation of a Hybrid Wind–PV–Pumped Storage Power System. *Energies* **2019**, *12*, 2809. [CrossRef]
23. Yan, Z.; Zhang, Y.; Liang, R.; Jin, W. An allocative method of hybrid electrical and thermal energy storage capacity for load shifting based on seasonal difference in district energy planning. *Energy* **2020**, *207*, 118139. [CrossRef]
24. Hemmati, R.; Shafie-Khah, M.; Catalao, J.P.S. Three-Level Hybrid Energy Storage Planning Under Uncertainty. *IEEE Trans. Ind. Electron.* **2019**, *66*, 2174–2184. [CrossRef]
25. Cheng, H.; Wu, J.; Luo, Z.; Zhou, F.; Liu, X.; Lu, T. Optimal Planning of Multi-Energy System Considering Thermal Storage Capacity of Heating Network and Heat Load. *IEEE Access* **2019**, *7*, 13364–13372. [CrossRef]
26. Khalid, M.; Akram, U.; Shafiq, S. Optimal Planning of Multiple Distributed Generating Units and Storage in Active Distribution Networks. *IEEE Access* **2018**, *6*, 55234–55244. [CrossRef]
27. Wang, Q.; Tan, Z.; De, G.; Pu, L.; Wu, J. Research on promotion incentive policy and mechanism simulation model of energy storage technology. *Energy Sci. Eng.* **2019**, *7*, 3147–3159. [CrossRef]
28. Zhou, T.; Kang, C.; Xu, Q.; Chen, Q. Preliminary Theoretical Investigation on Power System Carbon Emission Flow. *Autom. Electr. Power Syst.* **2012**, *36*, 38–43.

29. Kang, C.; Zhou, T.; Chen, Q.; Wang, J.; Sun, Y.; Xia, Q.; Yan, H. Carbon Emission Flow from Generation to Demand: A Network-Based Model. *IEEE Trans. Smart Grid* **2015**, *6*, 2386–2394. [CrossRef]
30. Chen, D. *Study on Factor Decomposition and Network Flow Analysis of Carbon Emission in Power System*; Zhejiang University: Hangzhou, China, 2016.
31. Sivanagaraju, S.; Satyanarayana, S. *Electric Power Transmission and Distribution Losses*; Pearson Education: Delhi, India, 2018.
32. Bialek, J. Tracing the Flow of Electricity. *IEE Proc. Gener. Transm. Distrib.* **1996**, *143*, 313–320. [CrossRef]
33. Li, Y.; Zhang, N.; Du, E.; Liu, Y.; Cai, X.; He, D. Mechanism Study and Benefit Analysis on Power System Low Carbon Demand Response Based on Carbon Emission Flow. *Proc. CSEE* **2022**, *42*, 2830–2841.
34. Yang, L.; Xu, Y.; Sun, H.; Zhao, X. Two-Stage Convexification-Based Optimal Electricity-Gas Flow. *IEEE Trans. Smart Grid* **2020**, *11*, 1465–1475. [CrossRef]
35. Zimmerman, R.D.; Murillo-Sánchez, C.E. MATPOWER User's Manual. 2021. Available online: https://matpower.org/docs/MATPOWER-manual.pdf (accessed on 19 May 2022).
36. Jamie McIntyre, B.B.; Seto, H.; Borchard, S. *Comparison of Lifecycle Greenhouse Gas Emissions of Various Electricity Generation Sources*; World Nuclear Association: London, UK, 2011.
37. Cheng, Y.; Zhang, N.; Zhang, B.; Kang, C.; Xi, W.; Feng, M. Low-Carbon Operation of Multiple Energy Systems Based on Energy-Carbon Integrated Prices. *IEEE Trans. Smart Grid* **2020**, *11*, 1307–1318. [CrossRef]
38. Cao, Y.; Wei, W.; Wu, L.; Mei, S.; Shahidehpour, M.; Li, Z. Decentralized Operation of Interdependent Power Distribution Network and District Heating Network: A Market-Driven Approach. *IEEE Trans. Smart Grid* **2019**, *10*, 5374–5385. [CrossRef]
39. Chen, C.M.; Wu, X.Y.; Li, Y.; Zhu, X.J.; Li, Z.S.; Ma, J.E.; Qiu, W.Q.; Liu, C.; Lin, Z.Z.; Yang, L.; et al. Distributionally robust day-ahead scheduling of park-level integrated energy system considering generalized energy storages. *Appl. Energy* **2021**, *302*, 117493. [CrossRef]
40. Shi, L.; Yang, F.; Liu, Y.; Wu, F. Multi-scenario user-side energy storage capacity optimization configuration considering social development. *Power Syst. Prot. Control* **2021**, *49*, 59–66.